Incorporating Nonlinear Solvent Response in Continuum Dielectric Models Using a Two-Sphere Description of the Born Radius

C. Satheesan Babu[†] and Carmay Lim*,[†,‡]

Institute of Biomedical Sciences, Academia Sinica, Taipei 11529, Taiwan R.O.C, and Department of Chemistry, National Tsing Hua University, Hsinchu 300, Taiwan

The charging free energy of a model diatomic molecule is studied with free energy simulations and continuum dielectric methods. A comparison of the two methods shows that continuum dielectric theory can successfully encapsulate the nonlinear solvent responses around the solute if the dielectric boundary is defined by $^{1}/_{2}(R_{atom,i} + R_{gmax,i})$, where $R_{atom,i}$ is the atomic radius of solute atom i, and $R_{gmax,i}$ is the first peak position of the solute atom−solvent atom radial number/charge density distribution function. Furthermore, continuum dielectric theory in conjunction with the two-sphere description of the dielectric boundary can reproduce simultaneously the electrostatic solvation free energies, as well as the solvent-induced electrostatic potentials and field components at the solute sites derived from simulations in the presence of explicit solvent.

Introduction

Continuum dielectric models for solvation assume that the polar solvent around a solute is a structureless continuous medium of dielectric constant ϵ.[1] Furthermore, they assume that the solvent-induced electrostatic potential at the solute site depends linearly on the solute charge qe. Consequently, the solvation free energy depends quadratically on the solute charge, as in the Born model:[2]

$$\Delta G^{Born} = \frac{-q^2 e^2}{2R}\left[1 - \frac{1}{\epsilon}\right] \tag{1}$$

In eq 1 R is the radius of the spherical solute cavity. Although eq 1 is derived assuming linear dielectric response of the solvent, in reality solvent molecules that interact strongly with the polar solute are highly structured, causing the solvent dielectric permittivity near the solute to be lower than the bulk value.[3−9] Thus, the solvent response cannot be "linear" in real molecular systems and the effects are collectively known as nonlinear dielectric responses.

For spherical systems the nonlinear responses of the solvent in continuum theory can be obtained from eq 1 either by adjusting R[10,11] or by finding appropriate distance-dependent functional forms for ϵ that can mimic the dielectric behavior of the solvent around the charge.[12−15] For molecular systems, the radii that determine the dielectric boundary are often treated as empirical variables. However, radii that have been adjusted to reproduce experimental hydration free energies based on continuum models often fail to reproduce the corresponding experimental entropies (i.e., the temperature dependence of the free energy)[16] as well as solvation free energies in non aqueous solvents.[17] These adjusted radii also fail to yield accurate solvent-induced electrostatic potentials and fields at solute charge sites, as shown by simulation and finite-difference Poisson studies on the hydration of a water molecule.[6] Thus, it is important to connect the radii that determine the dielectric

boundary to the molecular properties of the solute and solvent so that they represent the underlying physics of the system. However, most works on molecular solvation employing generalized Born models,[18] (or implicit solvation models) discuss various ways of varying these radii,[19−21] rather than providing a molecular basis for the adjusted radii.

The nonlinear responses of the solvent arise mainly from electrostriction and dielectric saturation.[3,4,6,22,23] Both effects originate from the same molecular phenomena but act in opposite directions. Strong solute−solvent interactions cause the solvent molecules to come closer to the solute charge, thus reducing the excluded volume of the solute (electrostriction). At the same time, they immobilize water orientations near the solute, thereby decreasing ϵ near the solute (dielectric saturation). The Born model with $R = R_{ion}$ (the bare ionic radius) incorporates the extreme effects of electrostriction since the solute volume cannot decrease beyond the ionic cavity as the ion is treated as a hard-sphere in the Born model (Figure 1a). The corresponding free energy, ΔG^{Born}_{ion} (with $R = R_{ion}$ in eq 1), *overestimates* the magnitude of the observed solvation free energy.[11,24] On the other hand, the Born model with $R = R_{gmax}$ (the first peak position of the ion−water oxygen or hydrogen radial number/charge density distribution function) incorporates the extreme effects of dielectric saturation since the solvent ϵ has decreased to unity in the annular space between the ion and the solvent (Figure 1b). In real systems, however, ϵ cannot decrease to unity due to solvent electronic polarization. The free energy, ΔG^{Born}_{gmax} (with $R = R_{gmax}$ in eq 1), *underestimates* the magnitude of the observed solvation free energy.[24]

Since R_{ion} and R_{gmax} describe the two molecular effects of the solvent around an ion, we tried a linear combination of the two radii to obtain an "effective" Born radius R_{eff} (i.e., $R_{eff} = aR_{ion} + bR_{gmax}$) that would incorporate the nonlinear responses of the solvent. By fitting the parameters a and b to the observed solvation free energies of ions, of crystal radii varying from 0.4 to 3 Å and charge varying from $-3e$ to $+4e$, R_{eff} was found to be well-approximated by the mean of R_{ion} and R_{gmax};[24] i.e.,

$$R_{eff} = (R_{ion} + R_{gmax})/2 \tag{2}$$

[†] Institute of Biomedical Sciences.
[‡] Department of Chemistry.

Continuum Dielectric Models

J. Phys. Chem. A, Vol. 105, No. 20, 2001 **5031**

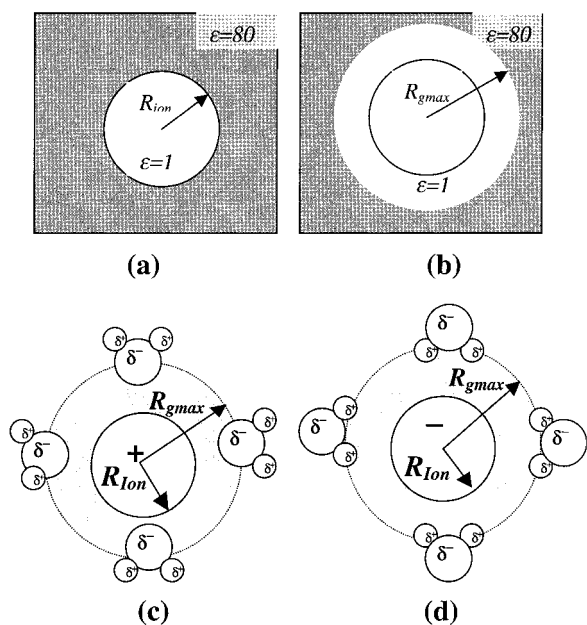**Figure 1.** A schematic diagram showing the Born model with (a) $R = R_{ion}$, the bare ionic radius, and (b) $R = R_{gmax}$, the first peak position of the ion−water oxygen or ion−water hydrogen radial number/charge density distribution function. The preferential orientation of water molecules around a cation and an anion are illustrated in (c) and (d), respectively.

Substituting eq 2 for R in eq 1 and rewriting the free energy in terms of the Born free energies of the bare-ion sphere ΔG_{ion}^{Born} and the solvated sphere ΔG_{gmax}^{Born} gives

$$\Delta G^{Corr} = \frac{2\Delta G_{ion}^{Born}\Delta G_{gmax}^{Born}}{\Delta G_{ion}^{Born} + \Delta G_{gmax}^{Born}} \qquad (3)$$

Eqs 2 and 3 have important implications. Equation 2 implies that R_{eff} can be derived from two well-defined and measurable distances around the ionic center; viz., the ionic radius and the solvation radius[14,25] *without any adjustable parameters*. On the other hand, eq 3 implies that a geometric combination of two "linear response" free energies (representing extreme electrostriction and dielectric saturation in the Born model) can take into account nonlinear solvent responses. Note that eq 3 is exact for spherical ions, but it is approximate for molecular solutes.[26]

It is important to note that the R_{eff} in eq 2 depends on the molecular nature of the solvent and the solution structure of the polar solute consistent with the thermodynamic state (temperature, pressure and composition of the solvent via R_{gmax}). It can reproduce not only experimental hydration free energies, but can also yield accurate hydration entropies and enthalpies of spherical ions[24] as well as solvation free energies of spherical ions in nonaqueous solvents such as dimethyl sulfoxide, acetonitrile and ethanol.[27] Furthermore, the "two-sphere" description of the effective Born radius could also be applied in continuum theories to compute the solvation of *non-spherical* molecules by replacing eq 2 with the following:

$$R_{eff,i} = (R_{atom,i} + R_{gmax,i})/2 \qquad (4)$$

where $R_{atom,i}$ is the atomic radius of solute atom i. By using eq 4 to define the dielectric boundary of model diatomic molecules of varying interatomic bond distances, hydration free energies obtained from finite-difference Poisson methods as well as Kirkwood and Generalized Born models were found to agree

with those derived from free energy simulations in the presence of explicit water molecules.[26]

Here, we verify that in continuum models, eq 4 incorporates the necessary nonlinear molecular solvent effects (see above) and yields fairly accurate predictions of electrostatic potentials and corresponding field components. To this end, we studied the charging of model $Na^{+q}-Cs^{-q}$ molecules with an internuclear bond distance of 3 Å and partial charge $q = 0.1, 0.3, 0.5, 0.7,$ and $1.0e$ in water. First, molecular dynamics (MD) simulations were carried out to determine the R_{gmax} of the solute atoms. Next, electrostatic solvation free energies and solvent-induced electrostatic potentials and field components at the solute charge sites were obtained from finite difference solutions to the Poisson equation using the "two-sphere" radius (eq 4) to define the dielectric boundary. These results were compared to corresponding results derived from molecular simulations with explicit solvent (ES). They were also compared to results obtained using the same theory (finite-difference Poisson methods) but with either R_{atom} or R_{gmax} (instead of their mean) in defining the dielectric boundary. Finally, the results from simulations and theory using the "two-sphere" radius (eq 4) were compared to those expected from a linear solvent response.

Methodology

Solvation Thermodynamic Cycle. The solvation free energy of a solute (ΔG^{solv}) can be thought of as a three-step process (Scheme 1).[6]

SCHEME 1
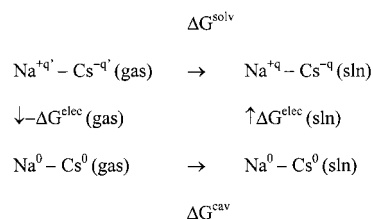
The first step involves discharging the solute in the gas phase; the corresponding free energy $-\Delta G^{elec}(gas)$ represents the free energy difference between the gas-phase molecule without and with partial charges. The second step involves solvating the uncharged solute; the corresponding free energy ΔG^{cav} is the work done to create the solute cavity in the solvent. The third step involves recharging the solute in solution; the corresponding free energy has two components: one due to the solute−solvent electrostatic forces $\Delta G^{elec}(sln)$ and the other due to the internal electrostatic energy of the solute in solution. The latter is generally assumed to cancel $-\Delta G^{elec}(gas)$ in (most) continuum dielectric models, which is not necessarily the case since the solute geometry and thus partial charges in the gas-phase and in solution need not be the same.[28,29] Furthermore, continuum calculations based on the Born model or numerical solutions to the Poisson equation neglect the ΔG^{cav} term. Hence, in these continuum calculations, the net $\Delta G^{solv} \approx \Delta G^{elec}(sln)$. The latter can be compared with the corresponding free energies derived from charging simulations of the molecule using a thermodynamic integration approach (see below).[30]

Force Field. The van der Waals (vdW) parameters for fully charged Na^+ and Cs^-, which have been calibrated to reproduce the experimental hydration free energies and ion−water distances of the isolated Na^+ and Cs^+ ions,[24,31] were assigned to the constituent atoms, Na^{+q} and Cs^{-q}, respectively. Such a choice removes ambiguity in the atomic radius since the ionic radii of Na^+ and Cs^- can now be used for the atomic radii in eq 4 as the vdW parameters for interaction with TIP3P water

have not been changed.[24] The simulations employed the TIP3P model of water whose oxygen and two hydrogen atoms form three sites with partial charges $q_O = -0.834e$ and $q_H = 0.417e$.[32]

MD Simulations. To estimate R_{gmax} of the solute atoms, constant volume MD simulations[33] of the model $Na^{+q}-Cs^{-q}$ molecules in TIP3P water[32] were performed using the CHARMM version27 program[34] at a mean temperature of 300 K. The solute was fixed at the center of a previously equilibrated cubic box of length 25.6 Å containing 560 water molecules at a density of 1 g/cc. Water molecules that overlapped with the solute atoms were removed by applying a distance criterion as in previous work.[24] This procedure resulted in the removal of one water molecule so that the final system contained 559 TIP3P water molecules and the diatomic solute. The simulations employed periodic boundary conditions and an atom-based *force*-switching function to smoothly switch the nonbonded forces to zero at 11.7 Å. The nonbond cutoff was set at 12.8 Å, which is half the length of the cubic simulation box, and the nonbond pair list was updated every 10 steps. The leapfrog Verlet algorithm was used with a time step of 2 fs. Each system was equilibrated for 20 ps and subjected to 100 ps of production dynamics, from which Na and Cs radial distribution functions (rdfs) were computed (see Simulation Analyses below).

Free Energy Simulations. Electrostatic solvation free energies of the model diatomic solutes were obtained from free energy simulations using the same simulation protocol as described in the previous section. The free energy for charging Na^0-Cs^0 to $Na^{+1e}-Cs^{-1e}$ was computed using thermodynamic integration with $\lambda = 0$ corresponding to the former ($q = 0$) and $\lambda = 1$ to the latter ($q = 1$). It is given by the integral:[30,35]

$$\Delta G^{elec}(sln) = \int_0^1 \langle dU^{elec}/d\lambda \rangle_\lambda \, d\lambda \qquad (5)$$

where the angular bracket indicates an ensemble average at λ. The average electrostatic energy is given by

$$\langle U^{elec} \rangle = \sum_{\alpha=1}^2 eq_\alpha \langle \Phi^\alpha \rangle \qquad (6)$$

where $\langle \Phi^\alpha \rangle$ is the solvent-induced electrostatic potential at position r_α of solute site α. The integration protocol employed 16 window points at $\lambda = 0, 0.1, 0.125, 0.2, 0.3, 0.4, 0.5, 0.6, 0.65, 0.7, 0.75, 0.8, 0.875, 0.9, 0.95,$ and 1. At each window point, the system was equilibrated for 10 ps, followed by 20 ps of production dynamics. Perturbation energies were collected every 4 fs for computing the relative free energies. The reverse perturbations were performed from a configuration that is independent from the forward perturbation runs. The free energies for the forward and reverse runs were then averaged. The free energies at intermediate charge states were extracted from the perturbation of the ($q = 0, \lambda = 0$) to ($q = 1, \lambda = 1$) state.

Simulation Analyses. The solvation radii R_{gmax} were computed from the first peak position of the atom-oxygen or atom-hydrogen rdfs $g(r)$, and used in eq 4 to compute R_{eff}, which in turn were employed to define the dielectric boundary in finite-difference Poisson calculations (see below). The rdfs were used to compute distance-dependent electrostatic potentials:[36]

$$\Phi^\alpha(R) = 4\pi \sum_X \rho_X \int_0^R \frac{q_X e}{r_{\alpha X}} g_{\alpha-X}(r) r^2 \, dr \qquad (7)$$

In eq 7, X denotes oxygen or hydrogen of TIP3P water, and the summation is based on charge density or charged particle

(P-summation).[37−40] If the summation scheme is based on group or molecule (M-summation) where water molecules are treated as groups,[6,7,37] the electrostatic potential at a distance R from the solute site α is computed from[37]

$$\Phi^\alpha(R) = \int_0^R dr \left\langle \sum_{i=1}^N \delta(r - r_{i,M}) \sum_X \frac{q_X e}{r_{aX}} \right\rangle \qquad (8)$$

In eq 8, N is the number of water molecules, $r_{i,M}$ is the distance between site α and the M center of the ith water molecule, $r_{\alpha X}$ is the distance between site α and the X atom (oxygen or hydrogen) of the ith water molecule, and the angular bracket denotes an ensemble average.

The electrostatic potentials from eqs 7 and 8 should be equal if all the charge in the system are considered. However, in computing pairwise interactions as well as in analyzing simulation trajectories, a spherical cutoff has to be used around the solute site α at less than or equal to half the length of the periodic cubic box. Such a spherical cutoff introduces significant differences in the potentials computed using eqs 7 and 8, typically 20 kcal/mol for a Lennard-Jones solute of the size of methane with a cutoff distance of 10 Å in water (with the oxygen of water as the M center in eq 8).[6,7] Since potentials based on charge-density summation (eq 7) have been shown to be incorrect,[38,41] the potentials here were computed using eq 8.

Note also that the potentials computed using eq 8 differ considerably for different choices of the molecular center.[37−40] Previous workers have shown that the dipole center of water is the theoretically correct choice,[38] and a physical meaning has been attributed to the existence of a molecular center for such potential calculations.[41] Hence, potentials were computed using eq 8 employing the dipole center of TIP3P water as the M center. It should be noted that the geometric center of TIP3P water is within 0.1 Å of its dipole center and thus the potentials and fields computed using these two centers are similar. The electric field components were obtained from the negative derivatives of the potentials.

Numerical Solution to Poisson Equation. The Poisson equation for the electrostatic potential $\Phi(r)$ at position r is given by

$$\nabla \cdot \epsilon(\mathbf{r}) \nabla \Phi(\mathbf{r}) + 4\pi\rho(\mathbf{r}) = 0 \qquad (9)$$

where $\rho(\mathbf{r})$ is the charge density and $\epsilon(\mathbf{r})$ is a position-dependent dielectric constant. The electrostatic potentials and fields at the solute sites due to the continuum solvent medium were obtained from finite difference solutions to the Poisson equation, as implemented in the Delphi program.[28,42] The calculations employed a 65 Å × 65 Å × 65 Å grid and a percentage grid fill of 80%. In conventional Delphi calculations a sphere of the same size as a water molecule is rolled over the solute surface, defined by the atomic coordinates and vdW radii of the solute atoms, to determine the low dielectric, solvent-inaccessible region. Such a procedure is not needed here since the definition of the effective Born radii (eq 4) incorporates the solvent accessibility.[26] The solute cavity was defined by eq 4, and the dielectric constant inside this cavity (ϵ_{in}) was set to 1 while that outside (ϵ_{out}) was set to 80, the dielectric constant of bulk water. Although the dielectric constant of TIP3P water is not 80 but approximately equal to 72,[43] this difference does not affect the results here as the electrostatic solvation free energy is not very sensitive to the external dielectric constant as long as it is large compared to unity (see eq 1).

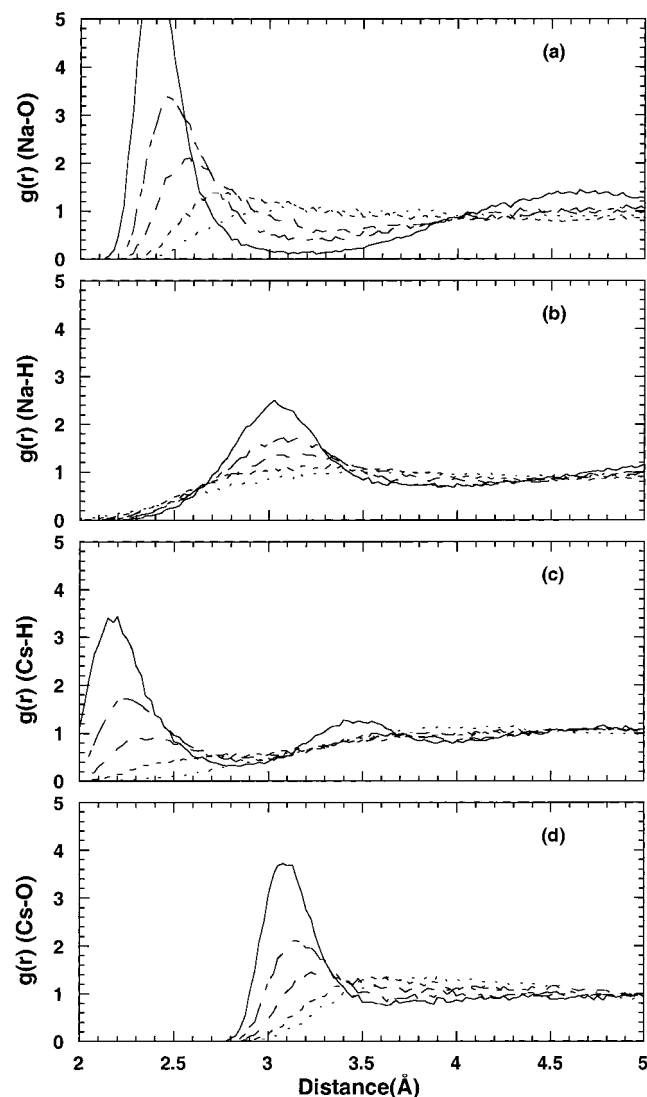The electrostatic potentials and fields were obtained from the differences in the respective quantities in aqueous solution (ϵ_{out}

Continuum Dielectric Models

J. Phys. Chem. A, Vol. 105, No. 20, 2001 **5033**

Figure 2. The solvation structure around the hypothetical polar Na^{+q}-Cs^{-q} solute at different charge states, as shown by (a) the Na—O rdf, (b) the Na—H rdf, (c) the Cs—H rdf, and (d) the Cs—O rdf. The solid curve (outermost first solvation peak) is for Na^{+}—Cs^{-} while the other curves in order of decreasing first peak height represent molecules with $q = 0.7, 0.5, 0.3,$ and $0.1e$, respectively.

= 80) and in the gas phase ($\epsilon_{out} = 1$). The electrostatic solvation free energies, ΔG_{CS} (where the subscript denotes continuum solvent) were obtained from similar differences in the reaction field energies. For comparison with ΔG_{CS}, electrostatic solvation free energies were also computed with the dielectric boundary defined either by the first peak of the atom-solvent rdfs or by rolling a water molecule over the solute surface defined by atomic radii.

Results and Discussion

Solvation Structure and Atomic Born Radii. Figure 2 shows how the solvation structural features of the Na^{+q}—Cs^{-q} molecules change as the charge q decreases from $1e$ to $0.1e$. The atom-solvent rdfs are all fully converged, but rdfs up to only 5 Å are depicted in the figures to show the characteristics of the first solvation shell that determine the effective Born radii. The atom-oxygen and atom-hydrogen rdfs for Na^{+}—Cs^{-} exhibit well-defined structural features with the first peak located at 2.38 Å for Na^{+} and 2.15 Å for Cs^{-}. As the field at the solute weakens (corresponding to Na^{+q}—Cs^{-q} molecules with $q < 1e$),

TABLE 1: The First Peak Position of the Solute-Oxygen (R_{gmax}^{O}) or Solute-Hydrogen (R_{gmax}^{H}) rdfs and Effective Born Radii (R_{eff}) of Na^{+qe}—Cs^{-qe} in Various Charge States^{a}

	Na			Cs		
$|q|$	R_{gmax}^{O}	R_{gmax}^{H}	R_{eff}^{b}	R_{gmax}^{H}	R_{gmax}^{O}	R_{eff}^{b}
0.1	3.05	3.18	2.02	2.88	3.90	2.27
0.3	2.70	3.18	1.84	2.68	3.55	2.17
0.5	2.58	3.08	1.78	2.40	3.23	2.03
0.7	2.45	3.08	1.72	2.25	3.15	1.95
1.0	2.38	3.03	1.68	2.15	3.08	1.90

^{a} All distances in angstroms. ^{b} Using eq 4 and $R_{atom,Na} = R_{ion,Na} = 0.98$ Å and $R_{atom,Cs} = R_{ion,Cs} = 1.65$ Å; the error in the computed effective radii are less than ± 0.03 Å.
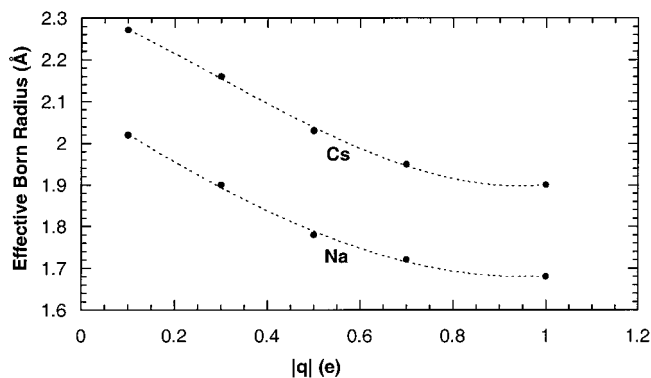

Figure 3. Effective Born radii R_{eff} as a function of charge (q/e) on the solute atoms. The dotted curves are cubic polynomial fits to the R_{eff} data points for Na and Cs.

the first peak of the atom-solvent rdf shifts to a longer distance, its height decreases while its width increases, reflecting weaker solute−solvent interactions. The solute atom-solvent distributions also reflect the orientational preferences of the water molecules around the positively and negatively charged sites of the molecule, as evidenced by the first peak positions of the atom-oxygen and atom-hydrogen rdfs (see Table 1). The water molecules orient with their oxygens pointing to Na^{+q} and their hydrogens pointing to Cs^{-q} (Figures 1c,d), thus the effective radii for Na^{+q} and Cs^{-q} are determined by the first peak positions of the Na−O and Cs−H rdfs, respectively (Table 1). Note that the Na−O and Cs−H rdf peak positions are the same as the corresponding Na−O and Cs−H charge density peak positions. The orientational preferences of water molecules around a charge become less important at large ion−water distances where the water−water interactions dominate. For example, the Born radii of cations and anions become equal when the sphere radius exceeds the length scale for which the ion−water interaction energy is comparable to the thermal energy.[44]

The Charge Dependence of the Effective Born Radii. Since the effective Born radius R_{eff} in eq 4 reflects the nature of the specific solute−solvent structures, it is determined by the charge of the solute as well as the molecular nature of the solvent; i.e., its molecular structure, composition and bulk solvent densities. In the present case, the different solvent surroundings are mainly due to the varying field from the molecule. This charge dependence is illustrated in Figure 3, where the R_{eff} for Na and Cs (black circles) in Table 1 are plotted as a function of charge, q/e. The dotted curves in Figure 3 represent best fits of the R_{eff} employing a cubic polynomial. The R_{eff} for Na and Cs decrease as the field at the solute increases irrespective of whether the site is positively charged or negatively charged. The observed decrease in R_{eff} reflects mainly the effects of electrostriction, where water molecules tend to *crowd* around the solute atom

TABLE 2: Electrostatic Solvation Free Energies (kcal/mol), Solvent-Induced Electrostatic Potentials (kcal/mol/e) and x Component of the Electric Fields (kcal/mol/e/Å) from Explicit Solvent (ES) Simulations and Continuum Solvent (CS) Models[a]

	ΔG			Φ at Na[b]		Φ at Cs[b]		E_x at Na[b]		E_x at Cs[b]	
$|q|$	ES	CS[c]	LR[c,d]	ES	CS	ES	CS	ES	CS	ES	CS
0.1	−0.4	−0.5	−0.6	−9.6	−6.1	1.8	4.4	2.5	2.8	2.2	2.6
	±0.1	(18%)	(43%)								
0.3	−5.0	−5.5	−5.3	−22.2	−22.3	13.4	14.8	9.5	9.2	7.8	8.6
	±0.3	(10%)	(7%)								
0.5	−15.9	−16.8	−17.0	−40.3	−39.6	27.7	28.7	16.5	16.3	14.8	15.4
	±0.3	(6%)	(7%)								
0.7	−34.3	−35.6	−36.3	−59.0	−59.2	44.6	44.0	26.2	23.4	24.4	22.6
	±0.4	(4%)	(6%)								
1.0	−76.7	−76.6	−80.5	−90.3	−88.7	70.7	66.9	36.8	34.3	33.9	33.2
	±0.4	(0.1%)	(5%)								

[a] The dielectric boundary is defined by eq 4 (see Methods). [b] The simulation numbers are computed from eq 8 with summation up to 10 Å and are based on the water molecule treated as a group with its dipole center as the molecular center (see Methods). [c] The numbers in brackets are the percentage deviation from the respective free energy simulation value. [d] The values are based on the linear response assumption; i.e., $\Delta G = (q^{Na}\Phi_{ES}^{Na} + q^{Cs}\Phi_{ES}^{Cs})/2$, where the potentials are obtained from explicit solvent simulations in columns 5 and 7.

as its charge is increased. However, as the solute charge is increased beyond 0.8e, the decrease in R_{eff} becomes negligible. The observed saturation in R_{eff} reflects the dominant effects of dielectric saturation at higher charge ($q > 0.8e$), where hydrogen-bonding and packing effects lock the orientation of the water molecules and prevent them from responding to further increase in solute charge. Such dependencies of the effective Born radius on solute charge have also been observed by other workers.[3,6,44]

Electrostatic Solvation Free Energies, Potentials, and Field Components. Table 2 gives the electrostatic solvation free energies ΔG, as well as the solvent-induced electrostatic potentials Φ and the x component of the solvent fields E_x at the solute sites for the $Na^{+q}-Cs^{-q}$ molecules in five charge-states. (The y and z components of the solvent fields at the solute sites are zero in theory but are nonzero in the simulations due to solvent packing.[6]) The statistical errors in the simulation free energies are estimated to be less than 0.5 kcal/mol (see Table 2). In addition, systematic errors in the simulation free energies due to the truncation of long-range electrostatic forces are generally nonnegligible. However, for the systems studied here, errors due to these effects are likely to cancel since the free energy difference between two states with the same net (zero) charge was computed; i.e., the $Na^{+q}-Cs^{-q}$ molecule was perturbed from $q = 0$ (net charge = 0) to $q = 1$ (net charge = 0). Such an expected cancellation of errors had been verified in our previous work[26] for $Na^{+0.5}-Cs^{-0.5}$ by performing two sets of calculations; viz., one with a spherical boundary of radius 20 Å and another with the same cubical periodic box as in this work. The two sets of free energies agree to within 5%.[26] On the other hand, errors in the R_{eff}, which are estimated to be about ±0.03 Å, yield corresponding uncertainties in the free energies obtained from finite-difference Poisson methods of less than 1%. Systematic errors in the electrostatic potentials and fields due to the truncation of long-range forces have been minimized by using a relatively large system and long nonbond cutoff. They are estimated to be less than ±2%.

Table 2 shows that Poisson equation with the two-sphere radius prescription for the dielectric boundary (eq 4) predicts electrostatic solvation free energies, as well as solvent-induced electrostatic potentials and field components at the solute sites in accord with respective simulation values. This is illustrated in Figure 4, where the simulation data points (filled circles) lie on or close to the solid lines, representing best fits to the theory results. Table 2 also shows that the agreement between electrostatic solvation free energies derived from theory and simulation improves with increasing solute charge/polarity: the
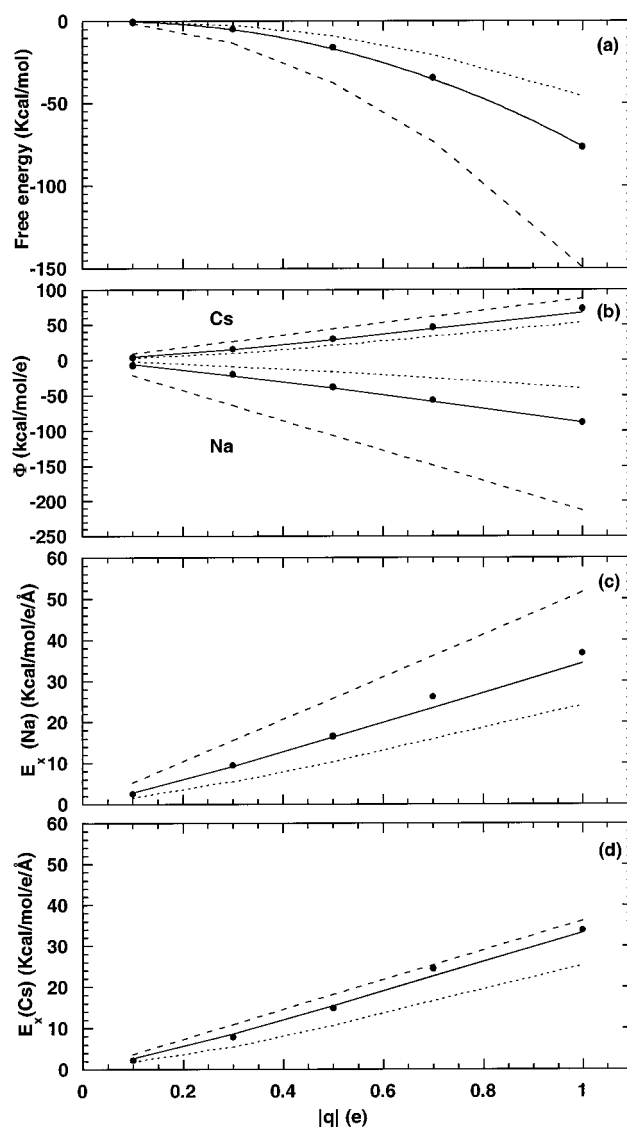

Figure 4. (a) The electrostatic solvation free energies, (b) solvent-induced electrostatic potentials at Na and Cs, (c) and the x component of the electric field at Na, and (d) Cs as a function of the charge q/e on the solute atoms. The filled circles are the simulation data points. The solid, dotted and dashed curves are best fits to the results obtained by solving Poisson equation with the dielectric boundary defined by R_{eff} (eq 4), by R_{gmax}, and by rolling a water molecule over the solute surface defined by R_{atom} (see Methods). In Figure 4b, electrostatic potentials at Cs are positive while those at Na are negative.

Continuum Dielectric Models

J. Phys. Chem. A, Vol. 105, No. 20, 2001 **5035**

percentage deviation of the continuum solvent free energy from the respective simulation value is 18% for $q = 0.1e$, 10% for $q = 0.3e$, 6% for $q = 0.5e$, 4% for $q = 0.7e$, and 0.1% for $q = 1e$. The same trend is generally found for the potentials and field components. A plausible reason for the observed trend is that the first solvation shells become more structured and the peak positions in the rdfs are better defined with increasing solute polarity (Figure 2). Note that nonlinear solvent effects stemming from electrostriction and dielectric saturation become dominant at higher solute polarity (see above). Therefore, the good agreement between theory and simulation results, especially for high solute charges, indicates that the two-sphere description of the atomic Born radii can capture these nonlinear solvent effects in continuum models.

Figure 4 compares the simulation (filled circles) and theory (solid line) results in Table 2 with corresponding results obtained by solving Poisson equation with the dielectric boundary defined either by R_{gmax} (dotted line) or by rolling a water molecule over the solute surface defined by R_{atom} (dashed line). Figure 4 shows that the dotted lines and dashed lines deviate from the respective simulation values and the deviations magnify with increasing solute polarity, in sharp contrast to the results obtained using eq 4 (solid line). Similar trends for the electrostatic solvation free energies were also observed for spherical ions and diatomic molecules of varying bond distances in previous works.[24,26] The present results indicate that the effective Born radius given by eq 4 appears to be unique in that it could yield fairly accurate electrostatic solvation free energies, potentials and fields unlike other choices for the effective Born radius. Figure 4 also shows that using R_{gmax} to define the dielectric boundary in finite-difference Poisson calculations[21,45] significantly *underestimates* the magnitude of the electrostatic solvation free energies, potentials and fields, hence care must be exercised in using such implicit solvent models in simulations.

Nonlinear Solvent Response. The linear response assumption means that the solvent-induced electrostatic potential at the solute atom center is a linear function of the solute charge; i.e., $\Phi_{LR} \approx k^{Na/Cs}qe$ (see Introduction). Therefore, the electrostatic solvation free energy is a quadratic function of the solute charge as in the Born model;[1,2] i.e., $\Delta G_{LR} \approx k(qe)^2 = (q_{Na}\Phi^{Na} + q_{Cs}\Phi^{Cs})/2$. The proportionality constants k^{Na}, k^{Cs}, and k were derived from the simulation results for $|q| = 1e$ since linear response is a better assumption when the solute fields are strong rather than weak (see Table 2). These constants were used to compute ΔG_{LR} and Φ_{LR} as a function of solute charge q/e (dotted curves in Figure 5). Figure 5 shows that the simulation results (represented by the solid curves) deviate from linear response behavior (dotted curves). Such deviations from linear response have also been observed for many real molecular solutes like water.[6,7] The observed nonlinear dependence of the potentials and nonquadratic dependence of the solvation free energies on the solute charge are successfully captured by the two-sphere description of the dielectric boundary in Poisson calculations, as evidenced by the closeness of the results (open circles in Figure 5) to the solid line.

It may seem surprising at first that "continuum" free energies, derived assuming linear solvent response, appear to account for nonlinear solvent effects if eq 4 is used to define the dielectric boundary. This is probably because they can be derived from two "linear response" free energies, as in eq 3 for spherical ions. To verify this, two sets of "linear response" free energies, ΔG^{CS}_{atom} and ΔG^{CS}_{gmax}, were obtained by solving Poisson equation with the dielectric boundary defined by R_{atom} and R_{gmax}, respectively. They were then combined as prescribed by eq 3.
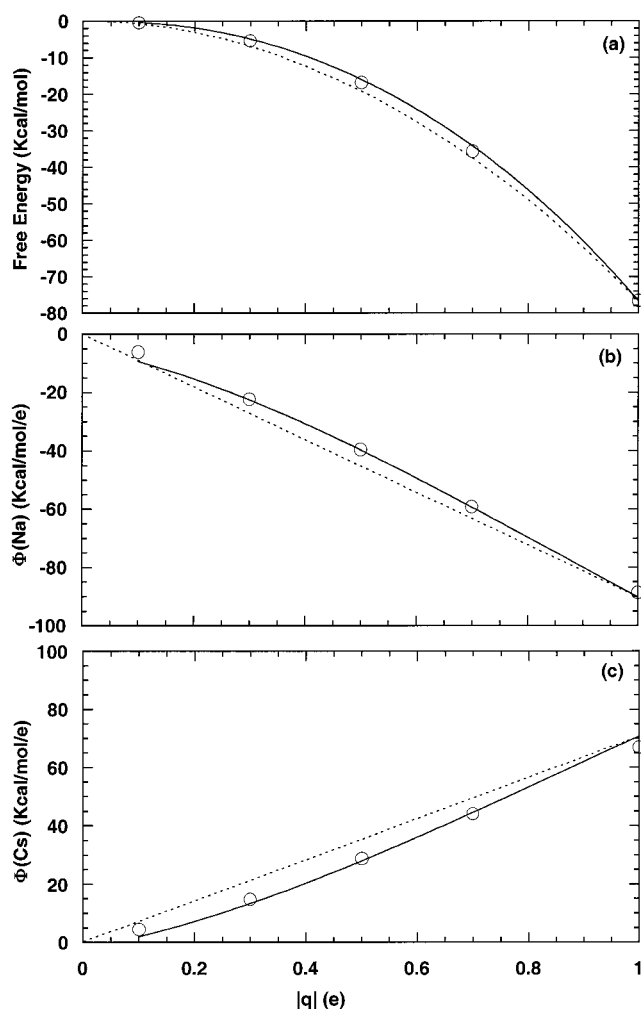

Figure 5. The deviations of the computed electrostatic (a) solvation free energies, and solvent-induced electrostatic potentials at (b) Na and (c) Cs from their linear response behavior. The solid curve is a third-order polynomial fit to the simulation data points. The open circles are data obtained from solving Poisson equation using eq 4 to define the dielectric boundary. The dotted curve is the behavior that is expected from a linear response of the continuum solvent; it is obtained from the force constant estimated from the simulation data for $|q| = 1e$ (see text).
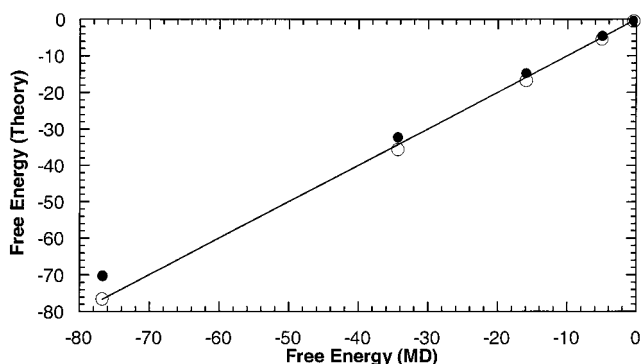

Figure 6. Plot of electrostatic solvation free energies obtained from simulation vs continuum theory. The solid line is the reference line, i.e., a plot of the simulation free energies vs itself. The open and filled circles are obtained by solving Poisson equation using eqs 4 and 3, respectively (see text).

Figure 6 shows that these free energies (filled circles) lie on or close to the solid line, which is a self-plot of the simulation free energies. However, the "continuum" free energies predicted using eq 3 are not as accurate as those predicted using eq 4

(open circles in Figure 6), especially as the solute polarity increases. The observed discrepancy is not unexpected as eq 3 is only approximate for nonspherical molecules since the presence of partial charges at atomic sites introduces a shielding contribution to the solvation free energy. Nevertheless, the results in Figure 6 suggest that, as for spherical ions, nonlinear solvent responses may be taken into account by some combination of two "linear response" free energies, ΔG_{atom}^{CS} and ΔG_{gmax}^{CS}. Note that our approach is based on a "purely" continuum model and is distinct from molecular theories based on a Gaussian form of the electrostatic potentials.[46,47]

Conclusions

The results here show that the solute radii that are used to define the dielectric boundary in continuum dielectric models can be defined by eq 4 to reflect the specific solution environment of the solute for a given thermodynamic state. The effective Born radii are determined by the solute charge (see Figure 3) as well as the solvent molecular structure, composition, and bulk density. By using eq 4 to define the dielectric boundary, continuum dielectric theory can reproduce simultaneously the electrostatic solvation free energies, as well as solvent-induced electrostatic potentials and field components at the solute sites obtained from simulations (to within 10% at high solute polarity, see Table 2). This was found not to be the case with other choices of effective solute cavity radii (see Introduction and Figure 4). In particular continuum dielectric theory using R_{gmax} (instead of $^1\!/_2 R_{gmax} + \,^1\!/_2 R_{atom}$) to define the solute cavity significantly *underestimates* the magnitude of the electrostatic solvation free energies, as well as the solvent-induced electrostatic potentials and field components at the solute sites (Figure 4). Furthermore, by using eq 4 to define the solute cavity, continuum dielectric theory can also incorporate the nonlinear solvent responses that are associated with charging a hypothetical diatomic solute in liquid water. This is evidenced in Figure 5, where the "two-sphere" theory results follow the simulation results in exhibiting a nonquadratic dependence on charge for the electrostatic solvation free energy and a nonlinear dependence for the electrostatic potential. The success of the two-sphere radius (eq 4) in capturing these nonlinear molecular effects is probably because it incorporates electrostriction and dielectric saturation in an averaged way in the continuum theory.

References and Notes

(1) Bottcher, C. J. F. *Theory of Electric Polarization*; Elsevier: Amsterdam, 1973.

(2) Born, M. *Z. Phys.* **1920**, *1*, 45−48.

(3) Jayaram, B.; Fine, R.; Sharp, K.; Honig, B. *J. Phys. Chem.* **1989**, *93*, 4320−4327.

(4) Roux, B.; Yu, H.-A.; Karplus, M. *J. Phys. Chem.* **1990**, *94*, 4683−4688.

(5) Friedman, H. L.; Raineri, F. O.; Xu, H. *Pure Appl. Chem.* **1991**, *63*, 1347−1356.

(6) Rick, S. W.; Berne, B. J. *J. Am. Chem. Soc.* **1994**, *116*, 3949−3954.

(7) Åqvist, J.; Hansson, T. *J. Phys. Chem.* **1996**, *100*, 9512−9521.

(8) Hyun, J.-K.; Ichiye, T. *J. Chem. Phys.* **1998**, *109*, 1074.

(9) Gavryushov, S.; Zielenkiewicz, P. *J. Phys. Chem. B* **1999**, *103*, 5860−5868.

(10) Voet, A. *Trans. Faraday Soc.* **1936**, *32*, 1301.

(11) Latimer, W.; Pitzer, K. S.; Slansky, C. M. *J. Chem. Phys.* **1939**, *7*, 108−111.

(12) Beveridge, D. L.; Schnuelle, G. W. *J. Phys. Chem.* **1975**, *79*, 2562.

(13) Abraham, M. H.; Liszi, J.; Meszaros, L. *J. Chem. Phys.* **1979**, *70*, 2491−2496.

(14) Marcus, Y. *J. Chem. Soc., Faraday Trans.* **1991**, *87*, 2995−2999.

(15) Hyun, J.-K.; Babu, C. S.; Ichiye, T. *J. Phys. Chem.* **1995**, *99*, 5187−5195.

(16) Noyes, R. M. *J. Am. Chem. Soc.* **1962**, *84*, 513.

(17) Friedman, H. L.; Krishnan, C. V. *Thermodynamics of Ionic Hydration*; Plenum Press: New York, 1973; Vol. 3.

(18) Still, W. C.; Tempczyk, A.; Hawley, R. C.; Hendrickson, T. *J. Am. Chem. Soc.* **1990**, *112*, 6127−6129.

(19) Dominy, B. N.; Brooks, III, C. L. *J. Phys. Chem. B* **1999**, *103*, 3765−3773.

(20) Jayaram, B.; Sprous, D.; Beveridge, D. L. *J. Phys. Chem. B* **1998**, *102*, 9571−9576.

(21) Nina, M.; Im, W.; Roux, B. *Biophys. Chem.* **1998**, *78*, 89−96.

(22) Bockris, J. O. M.; Reddy, A. K. N. *Modern Electrochemistry*; Plenum Press: New York, 1977; Vol 1.

(23) Conway, B. E. *Ionic hydration in Chemistry and Biophysics*; Elsevier: Amsterdam, 1981.

(24) Babu, C. S.; Lim, C. *J. Phys. Chem. B* **1999**, *103*, 7958−7968.

(25) Marcus, Y. *Chem. Rev.* **1988**, *88*, 1475−1498.

(26) Babu, C. S.; Lim, C. *J. Chem. Phys.* **2001**, *114*, 889−899.

(27) Madhusoodanan, M.; Lim, C. 2000. In preparation.

(28) Sharp, K. A.; Honig, B. *Ann. Rev. Biophys. Biophys. Chem.* **1990**, *19*, 310−332.

(29) Chan, S. L.; Lim, C. *J. Phys. Chem.* **1994**, *98*, 692−695.

(30) Beveridge, D. L.; DiCapua, F. M. *Free Energy via Molecular Simulation: A Primer*; ESCOM: Leiden, 1989.

(31) Åqvist, J. *J. Phys. Chem.* **1990**, *94*, 8021−8024.

(32) Jorgensen, W. L.; Chandrasekhar, J.; Madura, J. D.; Impey, R. W.; Klein, M. L. *J. Chem. Phys.* **1983**, *79*, 926−923.

(33) Allen, M. P.; Tildesley, D. J. *Computer Simulation of Liquids*; Oxford University Press: New York, 1990.

(34) Brooks, B. R.; Bruccoleri, R. E.; Olafson, B. D.; States, D. J.; Swaminathan, S.; Karplus, M. *J. Comp. Chem.* **1983**, *4*, 187−217.

(35) McQuarrie, D. A. *Statistical Mechanics*; Harper and Row: New York, 1976.

(36) Hansen, J. P.; McDonald, I. R. *Theory of Simple Liquids*; Academic Press:, 1986.

(37) Hummer, G.; Pratt, L. R.; Garcia, A. E.; Berne, B. J.; Rick, S. W. *J. Phys. Chem. B* **1997**, *101*, 3017−3020.

(38) Åqvist, J.; Hansson, T. *J. Phys. Chem. B* **1998**, *102*, 3837−3840.

(39) Hummer, G.; Pratt, L. R.; Garcia, A. E.; Garde, S.; Berne, B. J.; Rick, S. W. *J. Phys. Chem. B* **1998**, *102*, 3841−3843.

(40) Ashbaugh, H. S.; Sakane, S.; Wood, R. H. *J. Phys. Chem. B* **1998**, *102*, 3844−3845.

(41) Vorobjev, Y. N.; Hermans, J. *J. Phys. Chem. B* **1999**, *103*, 10234−10242.

(42) Nicholls, A.; Honig, B. *J. Comp. Chem.* **1991**, *12*, 435.

(43) Dang, L.-X.; Pettitt, B. M. *J. Phys. Chem.* **1990**, *94*, 4303.

(44) Ashbaugh, H. S. *J. Phys. Chem. B* **2000**, *104*, 7235−7238.

(45) Nina, M.; Beglov, D.; Roux, B. *J. Phys. Chem. B* **1997**, *101*, 5239−5248.

(46) Levy, R. M.; Belhadj, M.; Kitchen, D. B. *J. Chem. Phys.* **1991**, *95*, 3627.

(47) Hummer, G.; Pratt, L. R.; Garcia, A. E. *J. Am. Chem. Soc.* **1997**, *119*, 8523−8527.